

OH-chemistry of non-methane organic gases (NMOG) emitted from laboratory and ambient biomass burning smoke: evaluating the influence of furans and oxygenated aromatics on ozone and secondary NMOG formation.

Matthew M. Coggon^{1,2}, Christopher Y. Lim³, Abigail R. Koss^{1,2,†}, Kanako Sekimoto^{1,2,4}, Bin Yuan^{1,2,†}, Jessica B Gilman², David H. Hagan³, Vanessa Selimovic⁵, Kyle Zarzana^{1,2}, Steven Brown², James M. Roberts², Markus Müller⁶, Robert Yokelson⁵, Armin Wisthaler^{7,8}, Jordan Krechmer⁹, Jose Jimenez^{1,10}, Christopher Cappa¹¹, Jesse Kroll³, Joost de Gouw^{1,10}, and Carsten Warneke^{1,2}

¹Cooperative Institute for Research in Environmental Sciences, University of Colorado, Boulder, CO, USA

²NOAA Earth Systems Research Laboratory Chemical Sciences Division, Boulder, CO, USA

³Department of Civil and Environmental Engineering, Massachusetts Institute of Technology, Cambridge, MA, USA

⁴Graduate School of Nanobioscience, Yokohama City University, Yokohama, Kanagawa, Japan

⁵Department of Chemistry and Biochemistry, University of Montana, Missoula, MT, USA

⁶Ionicon Analytik, Innsbruck, Austria

⁷Institute for Ion Physics and Applied Physics, University of Innsbruck, Innsbruck , Austria

⁸Department of Chemistry, University of Oslo, Oslo, Norway

⁹Aerodyne Research, Inc., Billerica, MA, USA

¹⁰Department of Chemistry, University of Colorado, Boulder, CO, USA

¹¹Department of Civil and Environmental Engineering, University of California, Davis, CA, USA

[†]now Department of Civil and Environmental Engineering, Massachusetts Institute of Technology, Cambridge, MA, USA

[†]now at Institute for Environment and Climate Research, Jinan University, Guangzhou, China.

Correspondence: Matthew Coggon (matthew.m.coggon@noaa.gov), Carsten Warneke (carsten.warneke@noaa.gov)

1 Evaluating NMOG Wall Losses Through Tubing and Gas-Wall Partitioning

Prior to each small chamber experiment, the PTR-ToF-MS sampled NMOG directly from the stack, as described by Koss et al. (2018). To evaluate biases associated with NMOG transmission through the ductwork, we compare the distribution of NMOG measured from the stack with that inside the small chamber prior to the initiation of OH chemistry. Figure S15 shows the difference in NMOG profiles between small chamber and stack measurements (Small Chamber Bias = $[NMOG_i/CH_3CN]_{chamber} - [NMOG_i/CH_3CN]_{stack}$). We normalize the NMOG distribution to CH₃CN under the assumption the acetonitrile is not lost to surfaces. The top row shows bias histograms for three fires, while the bottom row shows a comparison between the normalized profiles with 1:1, 1:2, and 2:1 lines.

In general, most NMOG fall within 20% of the 1:1 line. Bias histograms (top row, Fig. S15) show that the NMOG/CH₃CN ratios are lower in the small chamber, which suggests that NMOG are lost to the ductwork; however, this loss appears to be normally distributed and not weighted towards any specific NMOG functionality. Some masses exhibit significantly higher

ratios with acetonitrile inside the small chamber (e.g. butenes, ethanol, formamide for F29); however, PTR-ToF-MS detection of these masses is poor due to contributions of fragments from higher masses (e.g. butene), or low sensitivity (e.g. ethanol).

Fig. S15 demonstrates that the NMOG distribution in the chamber is similar to the NMOG distribution sampled from the stack. These results are consistent with the conclusions drawn by Lim et al. (2019), which showed that the volatility distribution was not significantly different between stack and small chamber measurements.

2 Sensitivity of Modeled Secondary NMOG Formation to Furfural Branching Ratios

The reactions employed to represent furfural oxidation were estimated by Zhao and Wang (2017) via theoretical quantum chemistry calculations. To date, this mechanism has not been studied experimentally; consequently, the exact branching ratios of the three major pathways may differ from those used in this study (0.37 for channel A, 0.6 for channel B, and 0.03 for channel C, 6). Furfural plays a major role in the formation of secondary NMOG measured in the biomass burning plume described by Müller et al. (2016) and the assumed branching ratios may impact modeled formation of maleic anhydride, hydroxy furanone, and ozone.

Figure S16 shows model output of maleic anhydride, hydroxy furanone, and ozone for base case ($A = 0.37$, $B = 0.6$, $C = 0.03$), equal weight (0.33, 0.33, 0.33), and isolated channel (i.e., all channel A, B, or C) simulations of the biomass burning plume described by Müller et al. (2016). Overall, hydroxy furanone formation is most sensitive to the assumed branching ratio of channel B, which is the pathway that directly leads to hydroxy furanone formation (Fig. 6). Maleic anhydride is most sensitive to the assumed branching ratio of channel C; however, this sensitivity is weaker than that of hydroxy furanone since all pathways lead to a significant yield of maleic anhydride. The assumed branching ratios have little impact on ozone formation.

The sensitivity tests presented in Fig. S16 demonstrate the need for experimental evaluation of the furfural oxidation mechanism. This refinement may provide better constraints of important secondary NMOG; however, this will unlikely affect modeled ozone formation.

References

- Aschmann, S. M., Nishino, N., Arey, J., and Atkinson, R.: Products of the OH Radical-Initiated Reactions of Furan, 2- and 3-Methylfuran, and 2,3- and 2,5-Dimethylfuran in the Presence of NO, *J. Phys. Chem. A.*, 118, 457–466, 2014.
- Koss, A. R., Sekimoto, K., Gilman, J. B., Selimovic, V., Coggon, M. M., Zarzana, K. J., Yuan, B., Lerner, B. M., Brown, S. S., Jimenez, J. L., Krechmer, J., Roberts, J. M., Warneke, C., Yokelson, R. J., and de Gouw, J.: Non-methane organic gas emissions from biomass burning: identification, quantification, and emission factors from PTR-ToF during the FIREX 2016 laboratory experiment, *Atmospheric Chemistry and Physics*, 18, 3299–3319, <https://doi.org/10.5194/acp-18-3299-2018>, 2018.
- Lauraguais, A., Coeur-Tourneur, C., Cassez, A., Deboudt, K., Fourmentin, M., and Choël, M.: Atmospheric reactivity of hydroxyl radicals with guaiacol (2-methoxyphenol), a biomass burning emitted compound: Secondary organic aerosol formation and gas-phase oxidation products, *Atmospheric Environment*, 86, 155–163, 2014.
- Lim, C., Hagan, D., Cappa, C., Coggon, M. M., Koss, A. R., Sekimoto, K., de Gouw, J., Warneke, C., and Kroll, J.: Secondary organic aerosol formation from biomass burning emissions, *in prep.*, 2019.
- Müller, M., Anderson, B. E., Beyersdorf, A. J., Crawford, J. H., Diskin, G. S., Eichler, P., Fried, A., Keutsch, F. N., Mikoviny, T., Thornhill, K. L., Walega, J. G., Weinheimer, A. J., Yang, M., Yokelson, R. J., and Wisthaler, A.: In situ measurements and modeling of reactive trace gases in a small biomass burning plume, *Atmospheric Chemistry and Physics*, 16, 3813–3824, 2016.
- Sekimoto, K., Li, S.-M., Yuan, B., Koss, A., Coggon, M., Warneke, C., and de Gouw, J.: Calculation of the sensitivity of proton-transfer-reaction mass spectrometry (PTR-MS) for organic trace gases using molecular properties, *International Journal of Mass Spectrometry*, 421, 71–94, 2017.
- Zhao, X. and Wang, L.: Atmospheric Oxidation Mechanism of Furfural Initiated by Hydroxyl Radicals, *J. Phys. Chem. A.*, 121, 3247–3253, 2017.

Table S1. Rate constant parameters, photolysis frequency, and initial conditions for the species modeled in F26 and F38. Entries are ordered by mixing ratios measured during F38. Photolysis frequencies are calculated based on literature cross-sections, known/estimated quantum yields, and the scaled photon flux at 254 nm (4.5×10^{15} photons cm 2).

	MCM Name	k _{OH} (cm 3 molec $^{-1}$ s $^{-1}$)	k _{O₃} (cm 3 molec $^{-1}$ s $^{-1}$)	k _{NO₃} (cm 3 molec $^{-1}$ s $^{-1}$)	j (s $^{-1}$)	F26 (ppb)	F38 (ppb)
d-butanol	DBUTANOL	3.40E-12	0	0	0	37.26	44.86
Formaldehyde	HCHO	8.47E-12	0	5.50E-16	1.20E-05	14.07	17.84
1-butene	BUT1ENE	3.11E-11	1.06E-17	1.35E-14	0	4.53	13.84
Methanol	CH3OH	9.02E-13	0	0	0	22.23	11.79
Ethene	C2H4	7.74E-12	1.68E-18	2.24E-16	0	9.22	8.38
Acetaldehyde	CH3CHO	1.48E-11	0	2.84E-15	1.98E-05	15.44	7.86
Acetic Acid	CH3CO2H	8.00E-13	0	0	0	7.64	6.03
Ethyne	C2H2	7.46E-13	0	0	0	4.97	5.96
Formic Acid	HCOOH	4.50E-13	0	0	0	3.89	4.86
Acrolein	ACR	2.00E-11	2.90E-19	3.26E-15	3.86E-08	3.24	4.43
1-propene	C3H6	2.83E-11	1.04E-17	9.79E-15	0	7.52	2.64
2-furfural	FURFURAL	3.50E-11	0	0	1.34E-01	2.07	2.03
Acetone	CH3COCH3	1.78E-13	0	0	7.97E-05	5.60	1.95
Furan	FURAN	4.20E-11	0	0	0	2.26	1.87
Furanone	BZFUONE	4.45E-11	2.20E-19	3.00E-13	0	1.77	1.73
2,3-butanedione	BIACET	2.41E-13	0	0	2.55E-05	2.09	1.66
1,3-butadiene	C4H6	6.59E-11	6.64E-18	1.03E-13	0	2.40	1.42
Ethanol	C2H5OH	3.21E-12	0	0	0	1.63	1.34
Glyoxal	GLYOX	9.63E-12	0	2.84E-15	6.95E-05	0.98	1.25
Hydroxyacetone	ACETOL	4.42E-12	0	0	4.55E-05	1.30	1.12
Guaiacol	GUAIACOL	7.44E-11	0	0	0	2.94	1.10
5-methylfurfural	MEFURFURAL	5.10E-11	0	0	0	1.45	1.00
Catechol	CATECHOL	1.00E-10	9.20E-18	9.90E-11	0	1.45	1.00
Phenol	PHENOL	2.74E-11	0	3.80E-12	0	2.39	0.89
Methyl acetate	METHACET	3.50E-13	0	0	0	1.03	0.89
Propenoic acid	ACO2H	8.66E-12	0	0	0	0.87	0.86
Methyl vinyl ketone	MVK	1.99E-11	5.36E-18	0	8.06E-06	0.99	0.81

Table S1. (Continued)

	MCM Name	k_{OH} ($\text{cm}^3 \text{ molec}^{-1} \text{ s}^{-1}$)	k_{O_3} ($\text{cm}^3 \text{ molec}^{-1} \text{ s}^{-1}$)	k_{NO_3} ($\text{cm}^3 \text{ molec}^{-1} \text{ s}^{-1}$)	j (s^{-1})	F26 (ppb)	F38 (ppb)
o-cresol	CRESOL	4.65E-11	0	1.40E-11	0	2.58	0.79
alpha-pinene	APINENE	5.20E-11	9.53E-17	6.15E-12	0	0.76	0.78
Methyl glyoxal	MGLYOX	1.29E-11	0	6.82E-15	1.20E-04	0.69	0.69
Benzene	BENZENE	1.22E-12	0	0	0	1.93	0.67
2-methylfuran	MEFURAN	6.19E-11	0	0	0	1.35	0.64
Toluene	TOLUENE	5.59E-12	0	0	0	1.90	0.46
Isoprene	C5H8	9.91E-11	1.33E-17	7.03E-13	0	1.04	0.42
Methyl ethyl ketone	MEK	1.11E-12	0	0	4.55E-05	1.47	0.41
Acetic Anhydride	METHCOACET	1.00E-14	0	0	0	0.33	0.30
p-benzoquinone	PBZQONE	4.60E-12	0	3.00E-13	0	0.24	0.30
2,5-dimethylfuran	DIMEFURAN	1.32E-10	0	0	0	0.75	0.28
Methacrolein	MACR	2.84E-11	1.28E-18	3.40E-15	7.72E-08	0.29	0.24
Benzaldehyde	BENZAL	1.25E-11	0	2.40E-15	3.58E-04	0.28	0.19
2,3-dimethyl phenol	OXYLOL	8.00E-11	0	3.20E-11	0	0.71	0.16
Propenal	C4ALDB	3.40E-11	1.58E-18	6.00E-15	5.56E-08	0.18	0.15
Styrene	STYRENE	5.80E-11	1.70E-17	1.50E-12	0	0.36	0.11
1-pentene	PENT1ENE	3.10E-11	1.00E-17	1.20E-14	0	0.34	0.10
m-xylene	MXYL	2.31E-11	0	2.60E-16	0	0.26	0.09
p-xylene	PXYL	1.43E-11	0	5.00E-16	0	0.26	0.09
o-xylene	OXYL	1.36E-11	0	4.10E-16	0	0.17	0.06
Ethyl benzene	EBENZ	7.00E-12	0	1.20E-16	0	0.08	0.03
NO2	NO2	9.22E-12	3.72E-17	1.21E-12	5.05E-05	6.46	53.98
O3	O3	7.41E-14	4.96E-02	0	0	5.00	10.00
HONO	HONO	5.95E-12	0	0	5.90E-04	0.00	2.58
NO	NO	8.97E-12	1.78E-14	2.60E-11	0	0.08	0.40

Table S2. Calculated NMOG losses by reaction with OH, O₃, NO₃, and photolysis for F26, F38, and the ambient biomass burning plume described by Müller et al. (2016). All values are percentages of the integrated loss over 15 hr of atmospheric-equivalent OH oxidation. Entries are ordered according to the largest loss rates by each process, calculated for F38. Entries marked by a hyphen were not included in the modeling.

Primary Loss by OH

	F26				F38				Muller et al. (2016)			
	OH	O ₃	NO ₃	hν	OH	O ₃	NO ₃	hν	OH	O ₃	NO ₃	hν
5-methylfurfural	100	0	0	0	100	0	0	0	100	0	0	0
2,5-dimethylfuran	100	0	0	0	100	0	0	0	100	0	0	0
Guaiacol	100	0	0	0	100	0	0	0	—	—	—	—
Furan	100	0	0	0	100	0	0	0	100	0	0	0
2-methylfuran	100	0	0	0	100	0	0	0	100	0	0	0
Acetic Acid	100	0	0	0	100	0	0	0	100	0	0	0
Propenoic acid	100	0	0	0	100	0	0	0	—	—	—	—
Acetic Anhydride	100	0	0	0	100	0	0	0	—	—	—	—
Methanol	100	0	0	0	100	0	0	0	—	—	—	—
Benzene	100	0	0	0	100	0	0	0	100	0	0	0
Toluene	100	0	0	0	100	0	0	0	—	—	—	—
Ethene	100	0	0	0	100	0	0	0	97	3	0	0
Formic Acid	100	0	0	0	100	0	0	0	100	0	0	0
Ethanol	100	0	0	0	100	0	0	0	—	—	—	—
Methyl acetate	100	0	0	0	100	0	0	0	—	—	—	—
m-xylene	100	0	0	0	100	0	0	0	—	—	—	—
Ethyl benzene	100	0	0	0	100	0	0	0	—	—	—	—
o-xylene	100	0	0	0	100	0	0	0	—	—	—	—
p-xylene	100	0	0	0	100	0	0	0	—	—	—	—
Acrolein	100	0	0	0	100	0	0	0	—	—	—	—
Methacrolein	100	0	0	0	100	0	0	0	97	1	0	3
Propenal	100	0	0	0	100	0	0	0	—	—	—	—
1,3-butadiene	100	0	0	0	100	0	0	0	—	—	—	—
Ethyne	100	0	0	0	100	0	0	0	—	—	—	—
Isoprene	100	0	0	0	100	0	0	0	98	2	0	0
1-pentene	100	0	0	0	100	0	0	0	—	—	—	—
1-butene	100	0	0	0	100	0	0	0	—	—	—	—
1-propene	100	0	0	0	100	0	0	0	96	4	0	0
Methyl vinyl ketone	99	0	0	1	99	0	0	1	93	4	0	3
Furanone	100	0	0	0	99	0	1	0	100	0	0	0
Styrene	100	0	0	0	98	0	2	0	96	3	1	0

Table S2. (Continued)*Significant loss by NO₃*

	F26				F38				Muller et al. (2016)			
	OH	O ₃	NO ₃	hν	OH	O ₃	NO ₃	hν	OH	O ₃	NO ₃	hν
Catechol	93	0	7	0	66	0	34	0	82	1	17	0
o-cresol	98	0	2	0	83	0	17	0	94	0	6	0
2,3-dimethyl phenol	98	0	2	0	84	0	16	0	—	—	—	—
p-benzoquinone	99	0	1	0	91	0	9	0	—	—	—	—
Phenol	99	0	1	0	88	0	12	0	97	0	3	0
alpha-pinene	98	1	1	0	92	1	7	0	—	—	—	—

Significant loss by photolysis

	F26				F38				Muller et al. (2016)			
	OH	O ₃	NO ₃	hν	OH	O ₃	NO ₃	hν	OH	O ₃	NO ₃	hν
2-furfural	0	0	0	100	1	0	0	99	99	0	0	1
Acetone	18	0	0	82	16	0	0	84	77	0	0	23
2,3-butanedione	48	0	0	52	46	0	0	54	1	0	0	99
Methyl ethyl ketone	70	0	0	30	68	0	0	32	—	—	—	—
Benzaldehyde	74	0	0	26	73	0	0	27	—	—	—	—
Hydroxyacetone	93	0	0	7	91	0	0	9	88	0	0	12
Methyl glyoxal	93	0	0	7	91	0	0	9	—	—	—	—
Glyoxal	95	0	0	5	93	0	0	7	—	—	—	—
Formaldehyde	99	0	0	1	98	0	0	2	39	0	0	61
Acetaldehyde	98	0	0	2	98	0	0	2	95	0	0	5

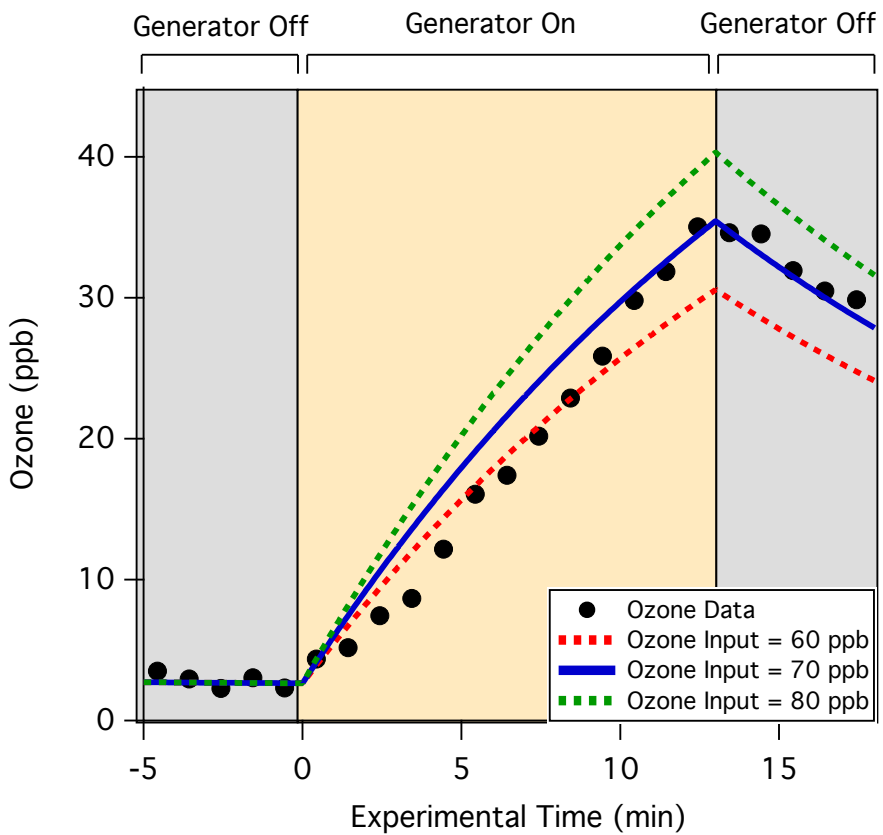


Figure S1. Modeled ozone compared to ozone measured during a dark, low NMOG (< 70 ppb) experiment. Output from the model is shown assuming that the dilution stream contains 60, 70, and 80 ppb of ozone. The input of ozone with the best fit (70 ppb) is applied to the photochemistry model described in Section 2.4

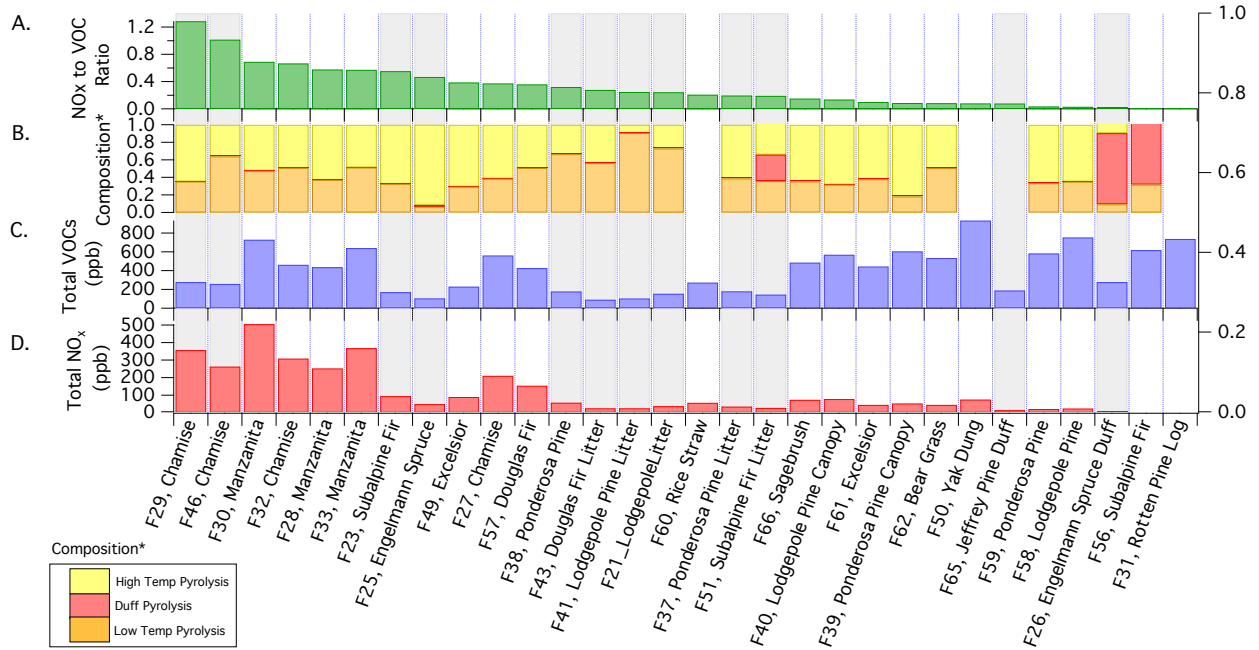


Figure S2. Small chamber (A) NO_x/NMOG ratio, (B) NMOG composition, (C) total NMOG loading, and (D) total NO_x prior to photochemical oxidation. Panel B shows the fraction of the total NMOG signal attributable to high temperature, low temperature, and duff pyrolysis as defined by Sekimoto et al. (2017). The grey bars indicate experiments in which initial NMOG loadings are sufficiently low to avoid significant OH titration.

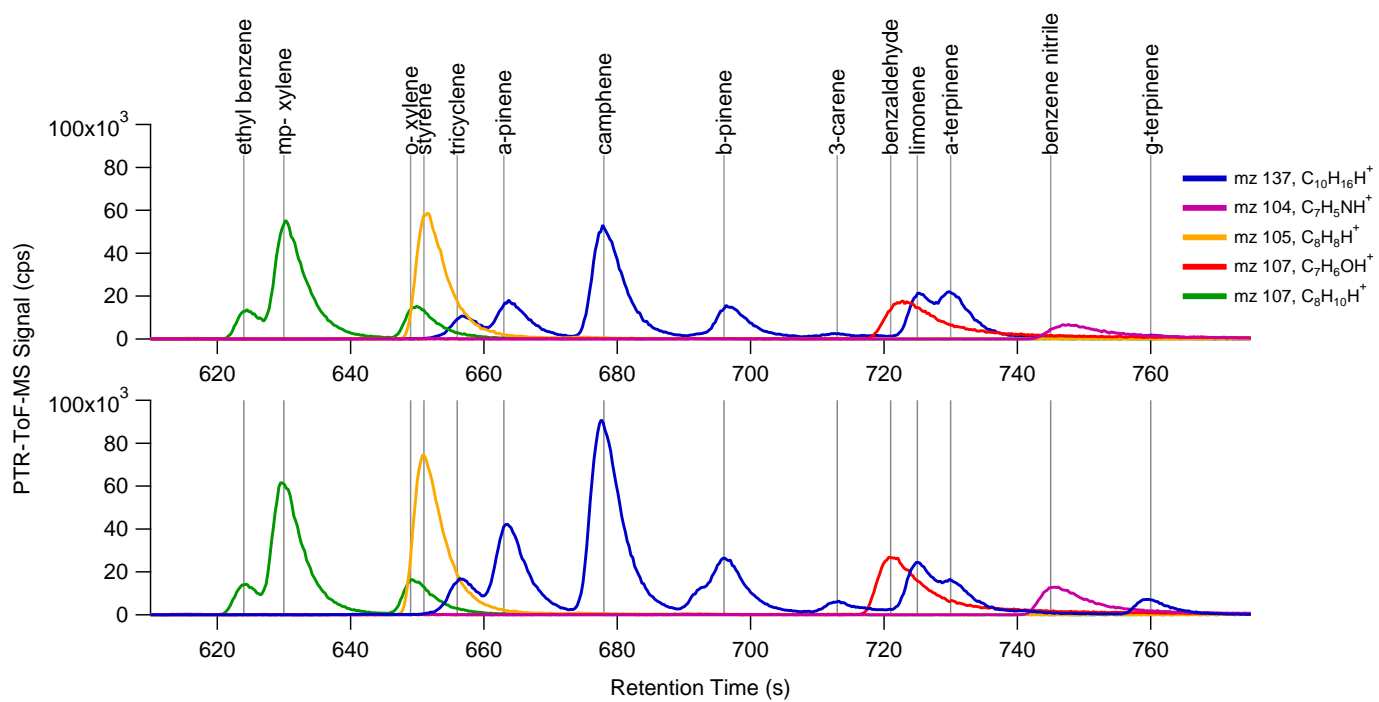


Figure S3. Distribution of monoterpenes (m/z 137) and other select NMOG measured from the combustion of douglas (top) and subalpine fir (bottom) using GC-PTR-ToF-MS.

Furan Reactions

— OH reactions
— RO₂ reactions
— Photolysis Reactions

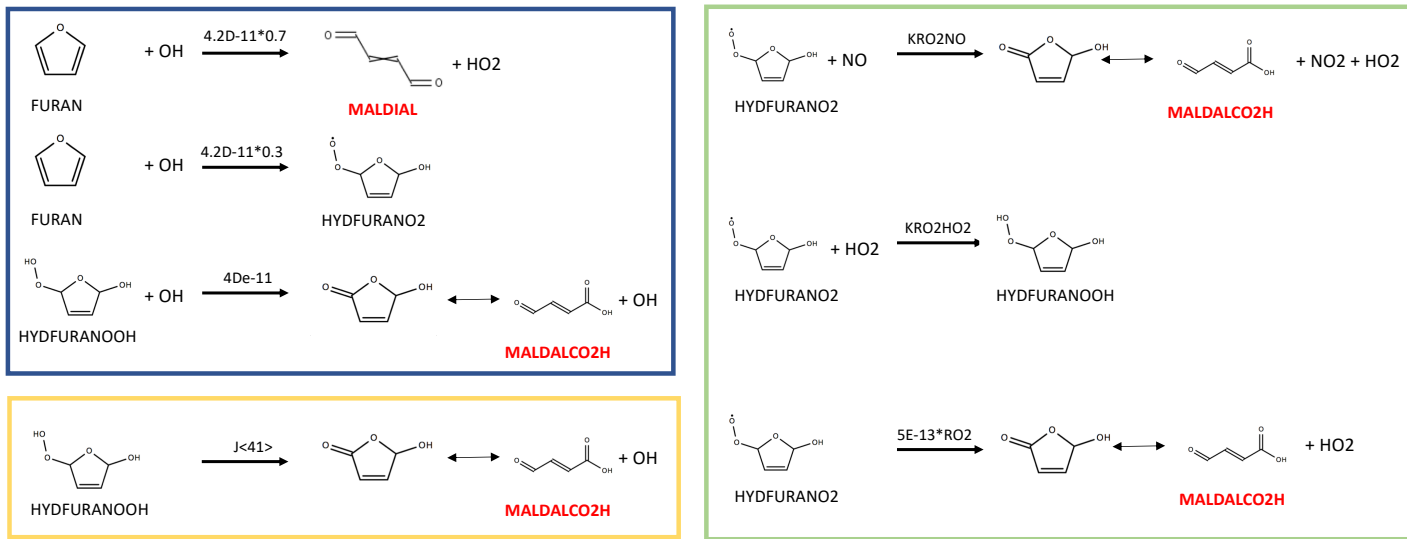


Figure S4. Furan reactions implemented into the MCM box model. Reactions are based on mechanism reported by Aschmann et al. (2014). Names in red indicate species currently represented in MCM v 3.3.1.

Methyl Furan Reactions

— OH reactions
— RO₂ reactions
— Photolysis Reactions

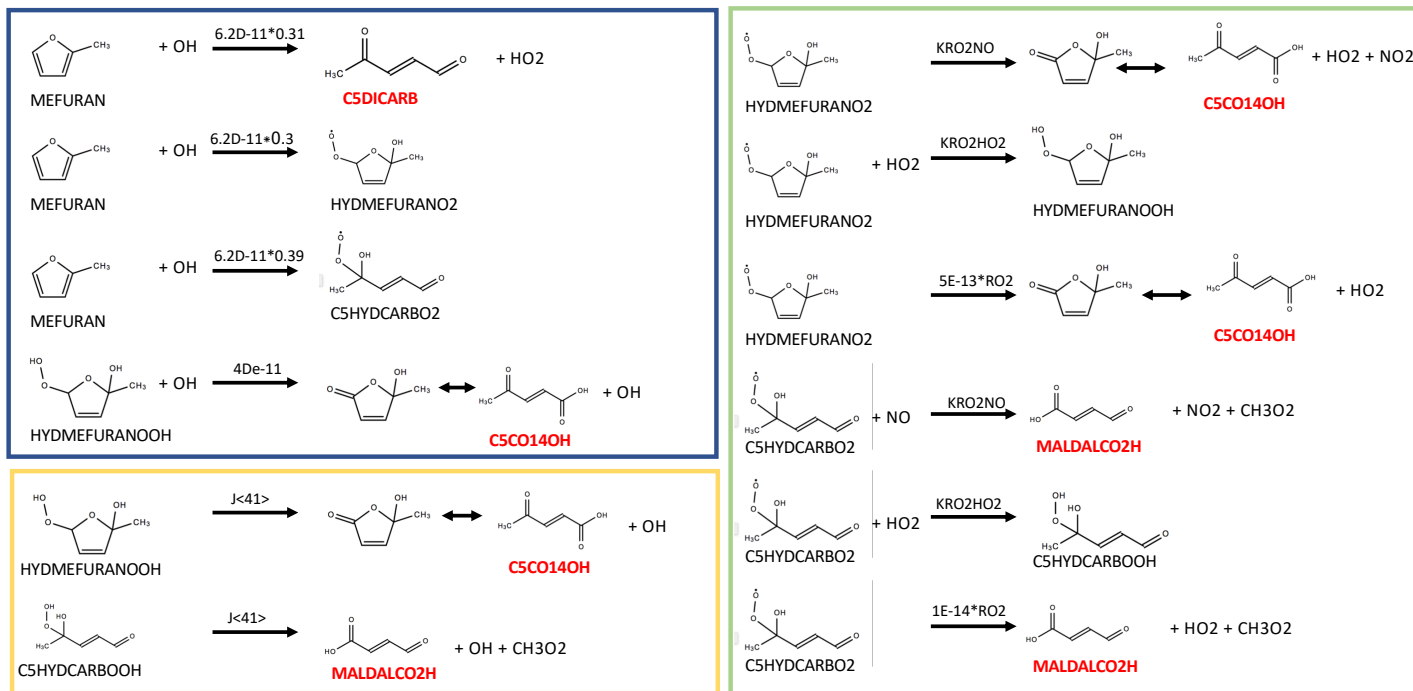


Figure S5. 2-methylfuran reactions implemented into the MCM box model. Reactions are based on mechanism reported by Aschmann et al. (2014). Names in red indicate species currently represented in MCM v 3.3.1.

Dimethyl Furan Reactions

— OH reactions
— RO₂ reactions
— Photolysis Reactions

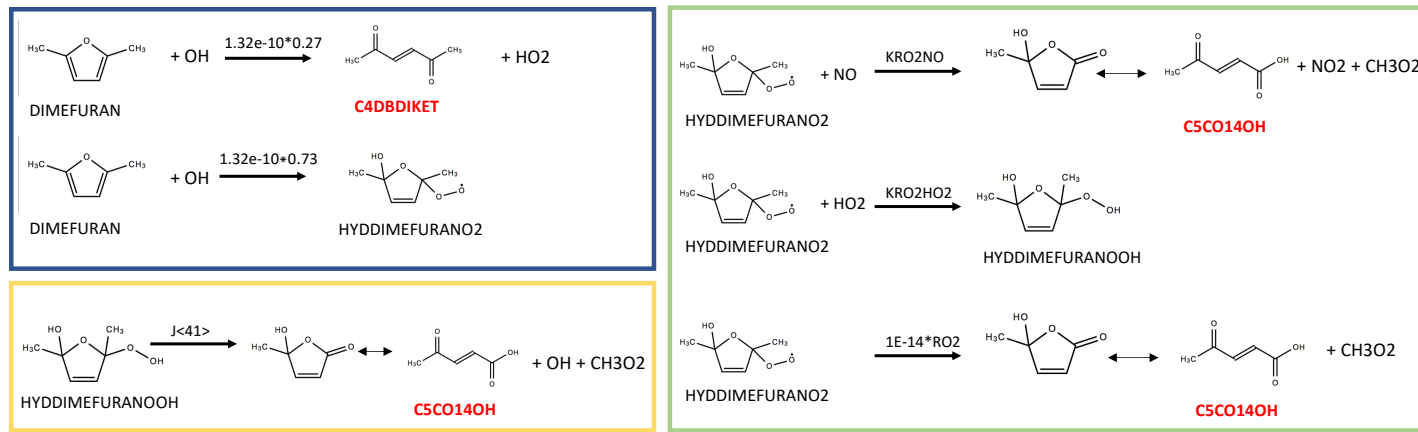


Figure S6. 2,5-dimethylfuran reactions implemented into the MCM box model. Reactions are based on mechanism reported by Aschmann et al. (2014). Names in red indicate species currently represented in MCM v 3.3.1.

Furfural Reactions

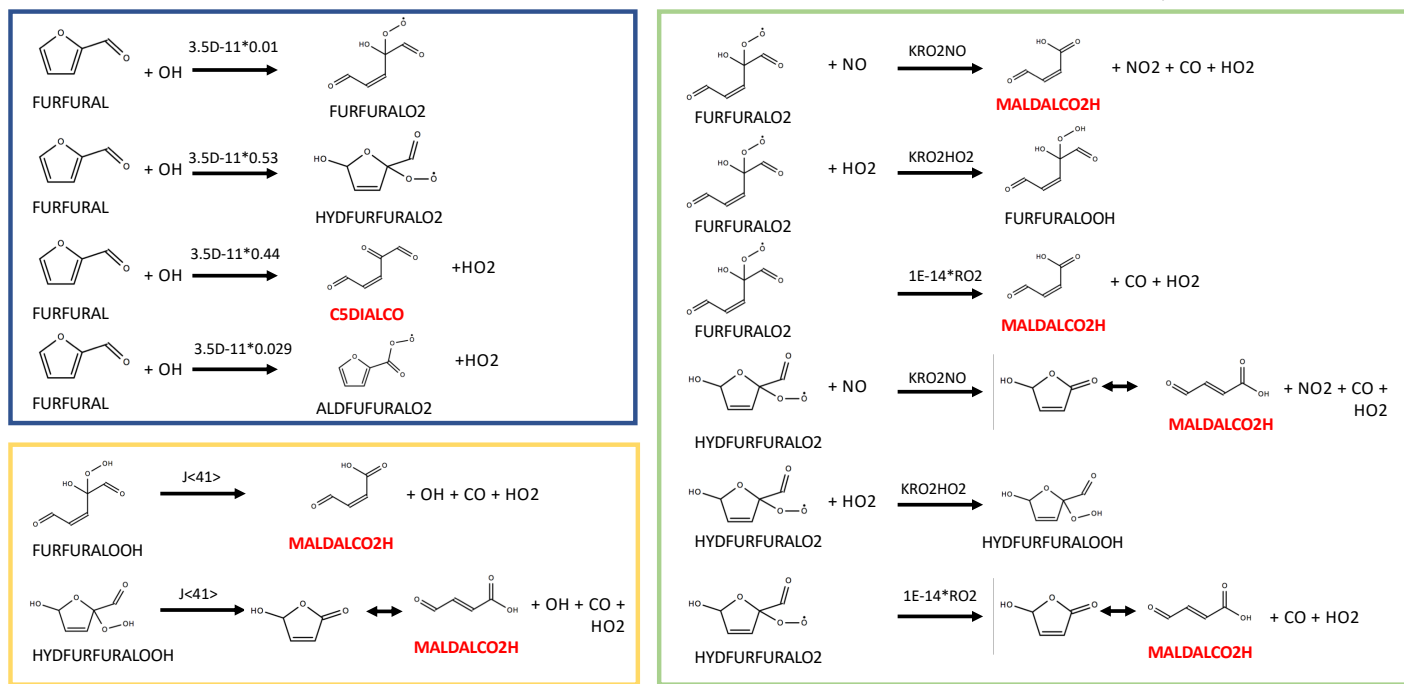


Figure S7. Furfural reactions implemented into the MCM box model. Reactions are based on mechanism reported by Zhao and Wang (2017). Names in red indicate species currently represented in MCM v 3.3.1.

Furfural Reactions (Continued)

— OH reactions
— RO₂ reactions
— Photolysis Reactions

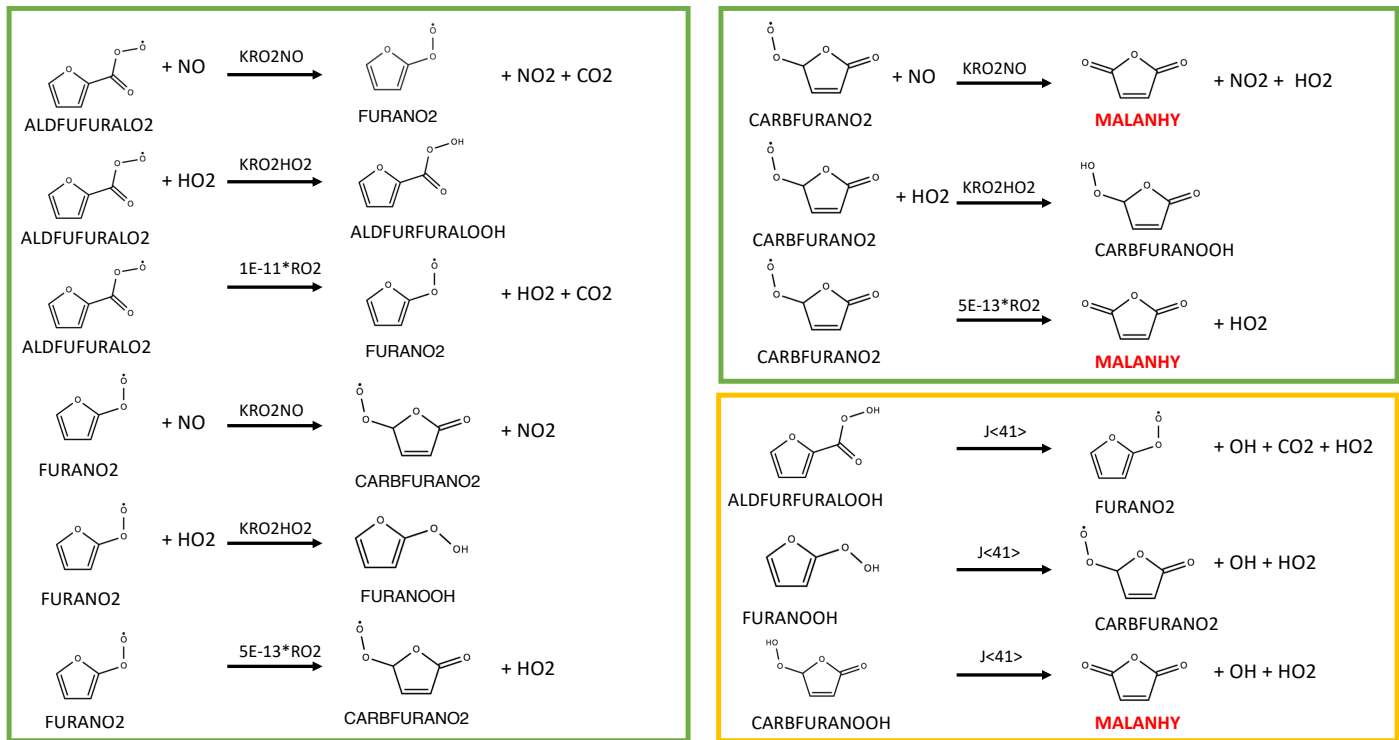


Figure S8. Furfural reactions implemented into the MCM box model (continued from Fig. S7s). Reactions are based on mechanism reported by Zhao and Wang (2017). Names in red indicate species currently represented in MCM v 3.3.1.

Methyl Furfural Reactions

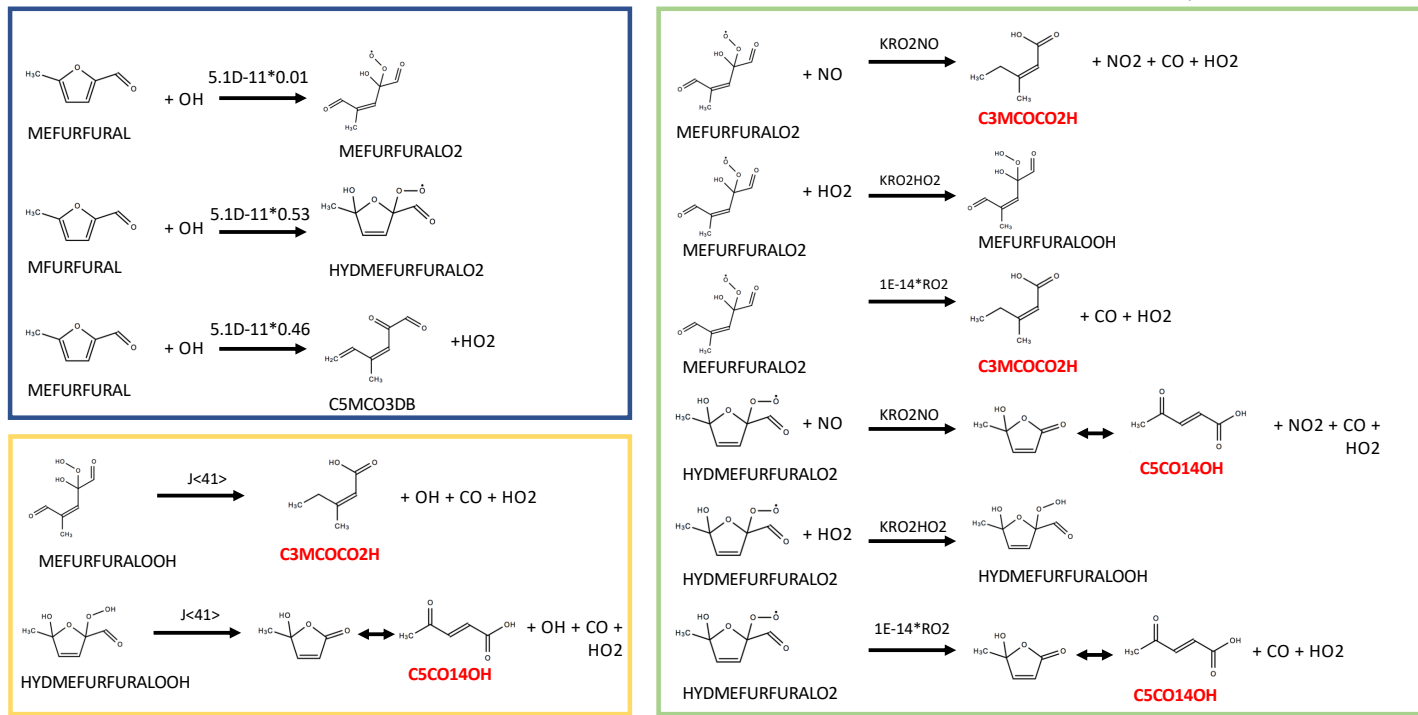


Figure S9. 5-methylfurfural reactions implemented into the MCM box model. Products and branching ratios are assumed to follow pathways analogous to the furfural mechanism reported by Zhao and Wang (2017). Names in red indicate species currently represented in MCM v 3.3.1.

Guaiacol Reactions

— OH reactions
— RO₂ reactions

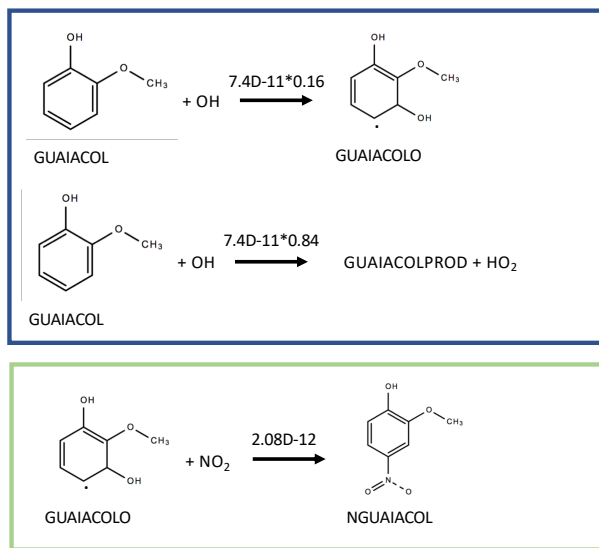


Figure S10. Guaiacol reactions implemented into the MCM box model. Reactions are based on the guaiacol mechanism reported by Lauraguais et al. (2014).

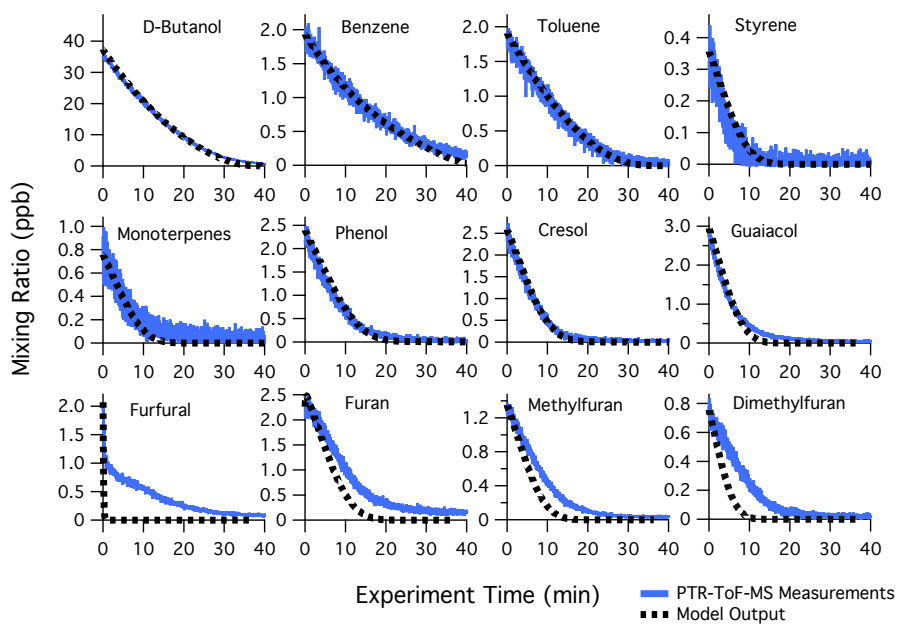


Figure S11. Primary NMOG measurements (blue lines) compared to modeled output (black dotted lines) for Fire 26. Fuel = Englemann Spruce Duff, $\text{NO}_x/\text{NMOG} = 0.02$, primarily duff pyrolysis NMOG mixture.

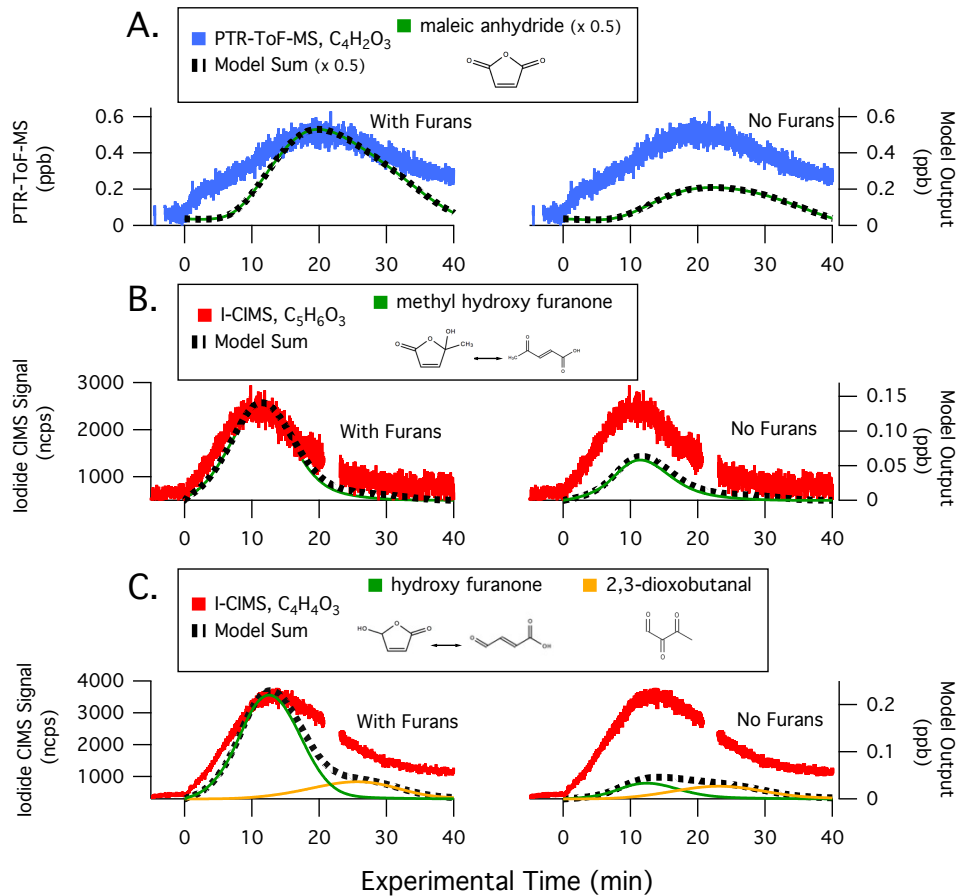


Figure S12. Secondary NMOG measurements compared to modeled output for Fire 26. Row (A) shows PTR-ToF-MS measurements of $C_4H_2O_3$ compared to model output of maleic anhydride. Row (B) shows I-ToF-CIMS measurements of $C_5H_6O_3$ compared to model output of methyl hydroxy furanone and its tautomer, β -acetyl acrylic acid. Row (C) shows I-ToF-CIMS measurements of $C_4H_4O_3$ compared to model output of hydroxy furanone, its tautomer malealdehydic acid, and 2,3-dioxobutanal. All graphs to the left show full model runs, while graphs to the right show model runs when the initial conditions of furan, 2-methylfuran, 2,5-dimethylfuran, furfural, 5-methylfurfural, and furanone are set to zero

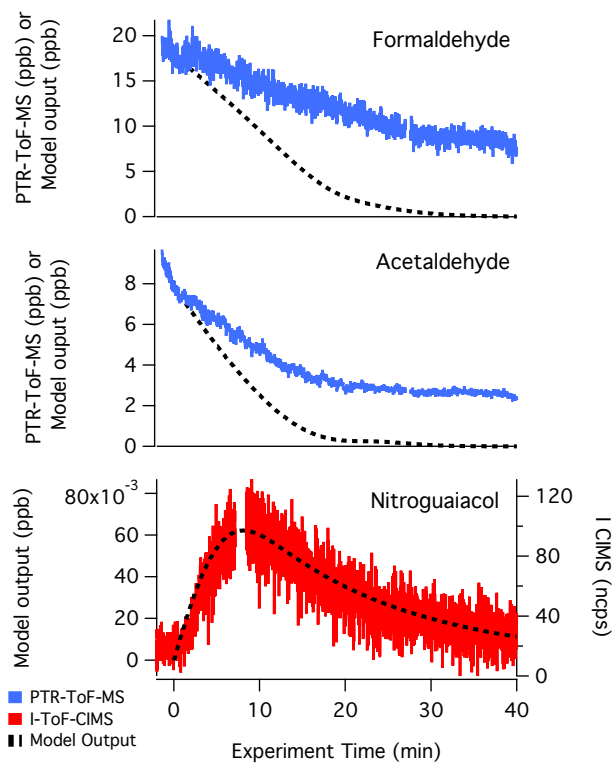


Figure S13. PTR-ToF-MS and I^- -ToF-CIMS measurements of formaldehyde, acetaldehyde, and nitroguaiacol compared to model output for F38.

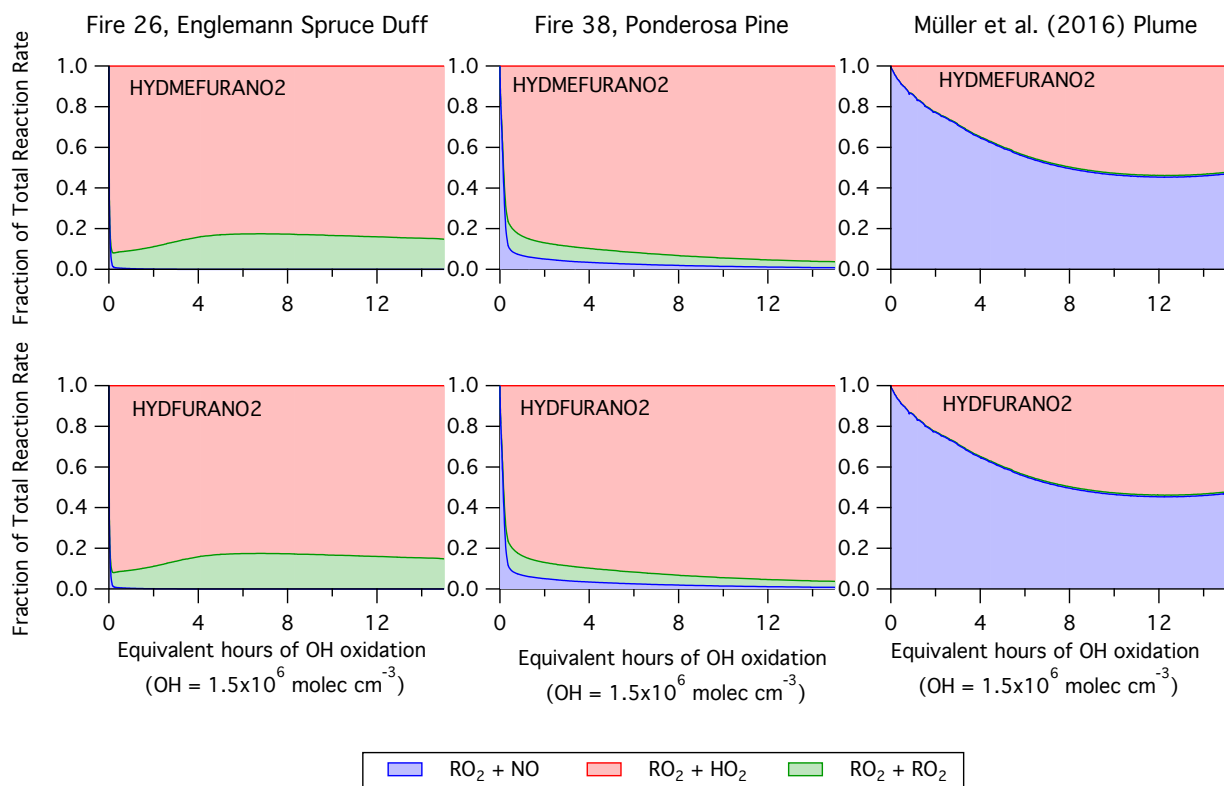


Figure S14. Fate of RO_2 species that lead to the formation of hydroxy furanone and methyl hydroxy furanone for F26, F38, and the ambient plume described by Müller et al. (2016). Shown is the fraction of RO_2 loss associated with reactions with HO_2 , NO , and other RO_2 radicals.

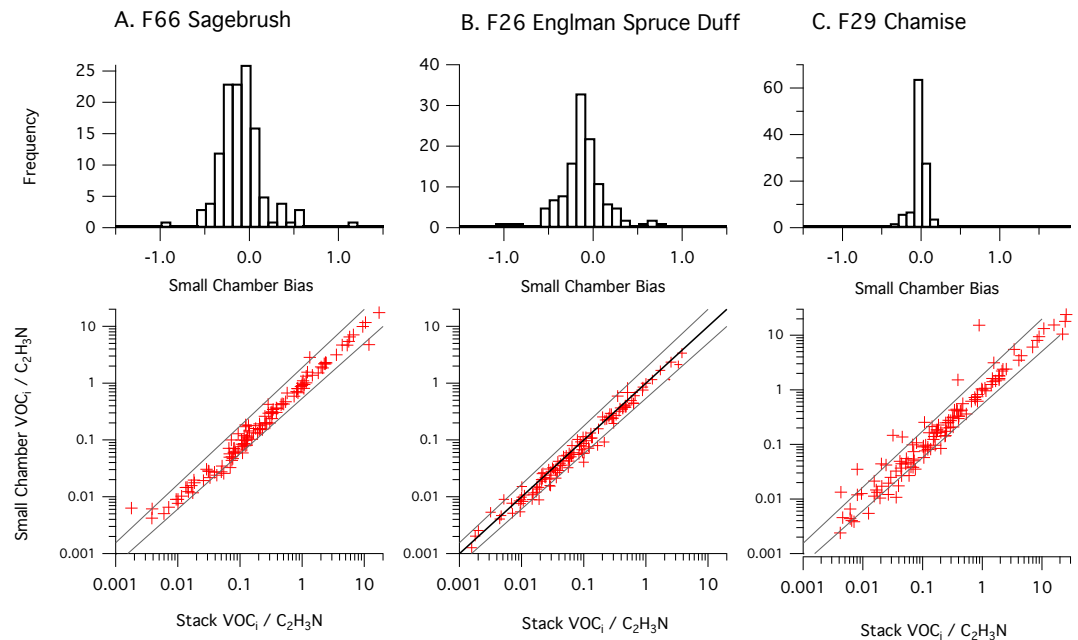


Figure S15. Comparison of NMOG distributions measured in the stack and small chamber prior to OH oxidation for (A) F66 - Sagebrush, (B) F26 - Englemann Spruce Duff, and (C) F29 Chamise. The bottom row shows the NMOG/C₂H₃N ratio for each species measured by the PTR-ToF-MS, along with 1:1, 2:1, and 1:2 lines.

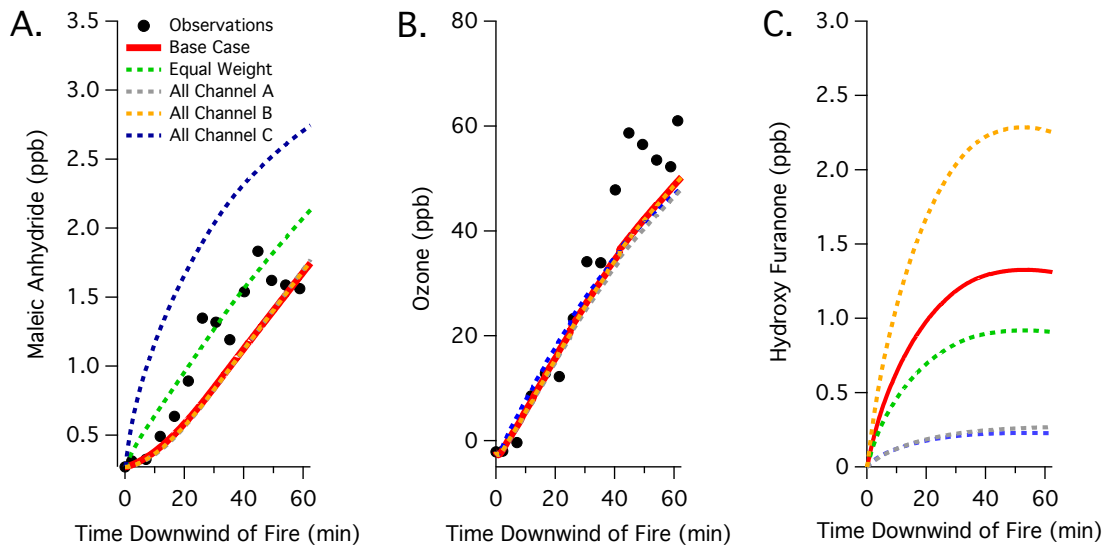


Figure S16. Model sensitivity of (A) maleic anhydride, (B) ozone, and (C) hydroxyfuranone to the assumed branching ratios of the furfural mechanism (Fig. 6). The "base case" simulation assumes branching ratios of $A = 0.37$, $B = 0.6$, $C = 0.03$ while the "equal weight" simulation assumes $A = 0.33$, $B = 0.33$, $C = 0.33$. All other simulations assume that furfural loss follows a single channel (i.e., all channel A, B, or C). Model output are compared to the measurements of maleic anhydride and ozone reported by Müller et al. (2016). Measurements of hydroxy furanone are not available.